

This is a postprint version of the following published document:

Juste, G. L., Sánchez De León, L., López-Núñez, E. & Fajardo, P. (2019). Sidewall effects on heat transfer in narrow backward facing step in transitional regime. *Numerical Heat Transfer, Part A: Applications*, 76(8), 628–647.




DOI: [10.1080/10407782.2019.1644930](https://doi.org/10.1080/10407782.2019.1644930)

© 2019 Taylor & Francis Group, LLC.



This work is licensed under a [Creative Commons Attribution-NonCommercial-NoDerivatives 4.0 International License](https://creativecommons.org/licenses/by-nc-nd/4.0/).

Sidewall effects on heat transfer in narrow backward facing step in transitional regime

Q5 G. L. Juste^a , L. Sánchez de León^a, E. López-Núñez  and P. Fajardo^c 

^aAerospace Propulsion and Fluid Mechanics Department, Universidad Politécnica de Madrid, Madrid, Spain; ^bIDR/UPM, Universidad Politécnica de Madrid, Madrid, Spain; ^cAerospace Engineering Group, Universidad Carlos III de Madrid, Leganés, Spain

ABSTRACT

In this work, we study numerically with large eddy simulation, the effects induced by the three-dimensional geometry of the channel on the flow topology that exists when the three-dimensional intrinsic instabilities appear in a backward facing step flow with low aspect ratio for Reynolds in the transitional regime ($Re = 1,000\text{--}1,600$), and its impact on the heat flux in the lower wall. Under the transitional regime, the three-dimensional instabilities begin to appear, but they can be masked by the flows due to the presence of the side walls. The study is carried out with two boundary conditions in the sidewalls, slip, and no-slip, to discriminate between the three-dimensionality induced by the geometry and the intrinsic three-dimensional instabilities. The results obtained are compared between the two boundary conditions, establishing what type of flow prevails and its influence on time-averaged mean Nusselt number for all Reynolds.

ARTICLE HISTORY



Received 3 May 2019
Accepted 12 July 2019

1. Introduction

The flow over a backward facing step (BFS) has been broadly studied since the 70s, both numerically and experimentally, with the aim of better understanding the physics of the flows with separation caused by sudden changes in the geometry and the succeeding adherence. This type of flow has implications for the heat transfer characteristics in numerous practical applications, such as the cooling of electronic equipment [1] and turbine blades [2, 3].

Pioneering studies, such as those by Denham and Patrick [4], Eaton and Johnson [5], and Armaly et al. [6] were focused on the study of basic characteristics of the flow (i.e., reattachment length and velocity field) in the different flow regimes (laminar, transitional, and turbulent) in two- or three-dimensional (2D, 3D) geometries with large aspect ratios (AR: channel width to step height ratio) of 35 and above.

Since then, a number of studies [7–10] have been conducted with two primary objectives: (1) acquire a deeper knowledge on various aspects of the isothermal flow over a BFS, such as the influence of the characteristic parameters of the problem, including Reynolds number (Re), channel expansion ratio (ER: duct height downstream of the step to step height ratio), and type of inflow, on the reattachment features and topology of the recirculation regions; and (2) analyze the 3D behavior of the flow because of the influence of the sidewalls. However, these studies typically considered 3D geometries with large ARs greater than 35.

CONTACT P. Fajardo  pablo.fajardo@uc3m.es  Aerospace Engineering Group, Universidad Carlos III de Madrid, Leganés, 28911, Spain.

Color versions of one or more of the figures in the article can be found online at www.tandfonline.com/unht.

© 2019 Taylor & Francis Group, LLC

Concerning the former objective, several works carried out have studied the relationship of the effects of the wall-jets originated by the existence of lateral walls and the sudden expansion of the flow, with the onset of flow unsteadiness [11, 12]. Iwai et al. [13] reported the influence of the channel AR on the 3D flow for the laminar regime ($Re = 250$). They concluded that the AR must be at least 16 to obtain a region of 2D flow in the center of the channel.

Looking at the 3D flow because of the effect of the sidewalls, Armaly et al. [14] and Nie and Armaly [15] reported on the flow in the laminar and the beginning of transitional regime on a channel with $AR = 8$. They report 3D flows because of the effect of the sidewalls, as the wall-jets, and a thinner upper recirculation zone adjacent to the sidewalls, modify the two-dimensionality of the flow. These jets produce a symmetrical reattachment line, with greater distances to the step in the sidewalls and center of the channel, and smaller in between.

For the same geometry (equal AR and ER), several authors [16–18] reported the effect of the lateral walls and analyzed the vortical structures that appear downstream of the step, associating them with Kelvin–Helmholtz instabilities and Taylor–Görtler vortices.

A characteristic phenomenon of the complex flow over the BFS is a fundamental 3D instability at a particular Re (bifurcation parameter), which is not because of the effect of the 3D geometry of the duct, but rather because of the first stages of the transition from a laminar and steady flow to a turbulent flow. When the bifurcation parameter reaches a critical value, vortical structures are formed. These flow structures initially grow with the bifurcation parameter and finally disappear, forming turbulent spots. The disintegration of large scales results in the transition from a stationary flow to a chaotic flow at the final stage, that is, turbulent flow.

A number of authors have conducted stability analyses of the flow over a BFS geometry. Relevant examples of these studies are those developed in references [19–25]. These references reported the critical Re for the primary global hydrodynamic instability, associated with a 3D bifurcation of the 2D flow for the same expansion ratio ($ER = 2$) as the study of Armaly et al. [14], and proposed that the centrifugal instability mechanism is responsible for generating 3D flows. To compare the values of the critical Re , it is worth noting that Barkley et al [20] defined the Reynolds number based on the maximum velocity at the step inlet and the step height, $Re_{sU_{max}}$, and not on the bulk inlet velocity and twice the channel height upstream of the step as other authors, Re_{2hU_b} . The relationship between them for $ER = 2$ is $Re_{sU_{max}} = 4/3 Re_{2hU_b}$.

Schäfer et al. [24] reported the transient behavior of the transitional flow ($Re_{2hU_b} = 6,000$) over a BFS with $ER = 2$ and considered periodic boundary conditions to remove the effect of the sidewalls. They reported an increase in the recirculation zone and the displacement downstream of the reattachment line over time. As time evolves, a region with negative velocity detached from the primary recirculation region and was convected downstream, therefore displacing upstream the reattachment line. This process created a self-sustained oscillation of the reattachment line. The authors suggested that this flapping motion of the reattachment line was related to the vortical structures of the unstable shear layer appearing between the main flow and the recirculation bubble.

Lanzerstorfer et al. [23] reported the global flow stability in a BFS geometry for different expansion ratios, assuming a homogeneous and infinitely extended configuration in the spanwise direction to study flow turbulent intrinsic effects, i.e., eliminating the effect of the sidewalls. They determined the critical Re as a function of the ER and proposed a mechanism for the instability. For $ER = 2$, they reported that the physical nature of the instability is not centrifugal, as proposed by Barkley et al. [20], but rather a combination of the flow deceleration, a lift-up process, and the convergence of the streamlines.

Both the 3D flows because of the sidewalls and the vortical structures because of the intrinsic flow instabilities affect the heat transfer process through the bottom wall downstream of the step.

Over the past decades, a number of researchers have focused their studies on the analysis of the bottom wall heat transfer characteristics for different flow configurations, both in 2D- and 3D-BFS geometries [26–29]. Chen et al. [30] reported a comprehensive review of these studies.

Recently, Xie and Xi [31] and Xie et al. [32] analyzed, using direct numerical simulation (DNS), the effect of the expansion ratio (in the range 1.5–2.5) and Re (based on the bulk inlet velocity and the step height, Re_{sUb}) on the flow and heat transfer characteristics on a 2D-BFS configuration. The authors also reported the effect of the vortical structures appearing downstream of the reattachment point in the transitional regime ($Re_{sUb} = 500$ – $1,200$), showing that these vortical structures improved the heat transfer characteristics.

Xu et al. [33] performed a similar study by means of URANS simulations in ANSYS-Fluent for incompressible flow in a 3D-BFS with $AR = 16$ and for a Re_{2hUb} in the range 200–1,400. The results indicate similar structures to those obtained by Xie et al. [32] in the midplane of the channel but yielded different values of the Strouhal number. The Nusselt number (Nu) distribution in the centerline exhibits secondary peaks because of flow fluctuations and associated instabilities.

The bulk of studies that focused on the analysis of the flow over a BFS under isothermal, adiabatic, or with heat transfer through the bottom wall conditions, were developed in 2D or 3D geometries for aspect ratios of 8 and above. Few authors have considered low aspect ratio geometries, such as those found in the internal cooling passages of turbine blades with ribs or the channels of heat sinks for electronic equipment, where the influence of the sidewalls reaches the midplane of the channel.

Barbosa et al. [34] reported the effect of the Richardson number in a BFS with $ER = 2$ and $AR = 4$ in a laminar regime ($Re_{2h} = 200$), obtaining notable differences between the mixed convection and forced convection flows. These differences affect the velocity field and the temperature distribution.

Iwai et al. [13] in their study of the effect of the AR on the flow configuration, simulated a case for $AR = 4$ and $Re = 250$, showing the variation of the Nu in the streamwise direction along the centerline of the channel, and its distribution on the bottom wall, highlighting the strong influence of AR on the Nu pattern, and that the maximum Nu appears close to the sidewalls and not on the centerline.

Avancha et al. [35] using large eddy simulation (LES), conducted a study of compressible flow on a BFS configuration with $AR = 4$ and $ER = 1.5$ for very low Mach numbers and Re_{sUmax} equal to 5540. They reported strong density fluctuations that can be associated to large temperature gradients and velocity fluctuations. The maximum Nu was found slightly upstream of the reattachment region. It was noted that the Reynolds analogy is not valid for the mean flow inside the recirculation zone for separated and reattached flows.

Finally, Zhao et al. [36] analyzed the effect of the Prandtl number in a BFS configuration with $AR = 4$ and $ER = 15$, using quasi-DNS for Re_{sUb} equal to 4,805.

Because of the limited number of studies in the literature dealing with narrow channels ($AR < 8$), the bulk of them considering laminar ($Re = 200$ – 250) or turbulent ($Re > 4,000$) regimes, the authors conducted a series of studies [37, 38] to better understand the effect of the sidewalls in narrow channels with BFS in laminar flow and the beginning of the transitional regime (Re_{2hUb} in the range 100–1,200). The first study [37] examined isothermal flow for a configuration with expansion ratio, $ER = 2$ and two aspect ratio (AR), 4 and 8, while the second one [38] considered heat transfer in the recirculation zone at the bottom wall under mixed-forced convection conditions for a configuration of $AR = 4$ and $ER = 2$. Simulations were performed using LES for ideal gas flow.

For the case where the effect of the side walls is eliminated through the no-slip boundary condition on the lateral walls, similar to the periodic boundary conditions used by other authors, it was shown that the flow features are a function of the spanwise position when intrinsic 3D instabilities appear, and that the distribution of the spanwise average Nu in the regions close to the

primary recirculation bubble is greater than the one obtained under the same flow conditions for no-slip case.

For the Re range analyzed in those studies, the effect of the sidewalls in narrow channels was dominant, damping the intrinsic 3D flow instabilities arising at the beginning of the transitional regime ($Re \sim 1,000$), leading to a symmetrical flow configuration. The result is that the mean Nu over the hot surface is greater in the case of slip sidewalls than for no-slip ones.

From previous results obtained by the authors, two significant issues arise: (1) up to what Reynolds number the effect of side walls dominates over intrinsic instabilities? and (2) which is its effect on heat transfer in the bottom wall? This study strives to answer these two questions for geometric configurations with low aspect ratio where the effect of the side walls extends to the center of the channel.

This study is organized as follows. Section 2 presents the description of the problem and the numerical model, similar to the one presented in [38]. Section 3 performs the sensitivity analysis for the largest Reynolds number studied in this work. Section 4 summarizes the validation of the numerical model. Section 5 presents and discusses the primary results obtained in the study.

Q1 Finally, Section 6 presents the key conclusions of this study.



2. Numerical model

2.1. Governing equations and numerical scheme

The problem addressed in this study is the forced convective flow over a 3D-BFS with low aspect ratio in the early transitional regime, i.e., Re in the range 1,000–1,600.

The equations that govern the problem are the Navier–Stokes equations for unsteady viscous flow of an ideal gas, in this case, air. In summary, these are the equations of continuity, momentum, and energy, together with the equation of state for the fluid.

In this analysis, flow Mach numbers are very low and, therefore, an incompressible formulation could be considered in the case of homogeneous and isothermal flows. However, when relevant heat transfer effects are present, causing significant temperature gradients in the wall, important changes in density occur because of thermal expansion and it is convenient to use a fully compressible formulation. For example, Avancha et al. [35] reported a numerical simulation with the LES approach and fully compressible formulation on a BFS with heat transfer at a Mach number of 0.006.

One of the problems of the computational fluid dynamics (CFD) methods applied to low Mach number flows is the excessive numerical dissipation and stiffness because of the wide disparity of time scales associated with the slower convection and with the rapid spread of waves. Pressure or acoustic waves or disturbances spread quickly through the domain, contaminating the solutions and, therefore, can weaken the stability of the scheme.

Several methods developed for the study of variable density low Mach number flows can be found in the literature. The methods are obtained either by modifying the density-based solvers for low Mach numbers, or by extending the pressure-based solvers towards this regime [39–41].

A common approach used to avoid the problems mentioned above is to separate the pressure, P , into a thermodynamic or operating pressure, P_{op} , and a hydrodynamic or relative part, p , which, for flows with small Mach numbers, is significantly lower than the operating pressure [41].

In spite of the low Mach numbers, to take into account the possible compressibility effects described above, in this study the ideal gas model has been adopted according to the formulation followed by the commercial code ANSYS-Fluent, where, the equation of state for the fluid (the ideal gas equation for air) in the pressure-based solver for the compressible flow of an ideal gas is defined as

$$\rho = \frac{P_{op} + p}{R_g T} \quad (1)$$

where ρ and T are the air density and temperature, respectively, R_g is the gas constant, P_{op} is the operating pressure, and p is the relative pressure at the considered location.

As mentioned above, the cases studied correspond to the early transitional regime, i.e., Re in the range 1,000–1,600. Typically, URANS approximations with high-order turbulence models could be inaccurate when predicting the flow mechanisms and the heat transfer characteristics in flows with separation and reattachment in the transitional regime, or in the turbulent regime without an adequate tuning of the turbulence models.

DNS solves all turbulent scales, spatially and temporally, so it can reveal fundamental aspects of the flow physics and provide details that cannot be obtained with classic URANS models, but at a much higher computational cost.

An intermediate solution is the use of LES, a numerical method where the transient and 3D movement on grid scales is explicitly calculated and the effects of non-linear interactions with the smallest, isotropic, and the bulk of universal scales are modeled using a sub-grid scale model. The separation of large eddies from small ones is achieved by filtering the Navier–Stokes flow equations. LES only solves turbulent scales from the largest to the inertial scale on the grid scales and, therefore, it does not have such a high computational cost as DNS for this type of separated and reattached flows that can be found in a BFS or, for that matter, in the internal cooling channels of turbine blades with ribs. These flows are dominated by large turbulence scales, which are of the order of the height of the step or rib [42].

LES is an affordable approach to obtain results with a high degree of reliability in these types of flows, where both laminar and transitional regimes are present [43, 44], as well as for the description of complex heat transfer mechanisms in forced or mixed-forced convective flows [3] with a moderate computational cost. For this reason, LES has been used by the authors in previous studies [37, 38] to analyze the influence of the sidewalls on the flow structure and the heat transfer characteristics in mixed-forced convective flows over a low aspect ratio BFS, and it is also the approach used in this study.

In LES of compressible flows, the filtered variables are weighed by the density, resulting in the Favre-averaged form of the equations. The complete detail of the spatially filtered equations in a Cartesian coordinate system can be found in the references [45, 46].

Among the existing LES models, the Dynamic Smagorinsky developed by Germano et al. [47] and Lilly [48] has been used relatively successfully for the study of rotating and non-rotating ribbed ducts [49]. These studies obtained results with 10–15% accuracy when compared against the quasi-DNS techniques and 15–30% (depending on the resolution of the mesh) when compared against experimental results, significantly improving the predictions obtained by RANS models.

For this reason, although the Dynamic Smagorinsky model was developed in 1991, and there are other existing SGS models nowadays, this analysis was performed using a Dynamic Smagorinsky model. As mentioned above, the simulations were conducted using the commercial CFD code ANSYS-Fluent [50], in which the Dynamic Smagorinsky formulation is executed using the development of Kim [51]. Moreover, the model has been confronted with the results obtained with open source DNS code [52], for the same geometrical configuration, in the case of adiabatic flow of an ideal incompressible gas for $Re = 1,200$. An example is shown in Figure 1, where the reattachment line obtained with both codes is successfully compared. Thus, validating the computational model.

The setup of the numerical model can be seen in [38, 50]. The transient formulation was carried out with a non-iterative time-advancement scheme, and a small time step ($1E-6$) to ensure a numerically stable solution together with efficient calculation.

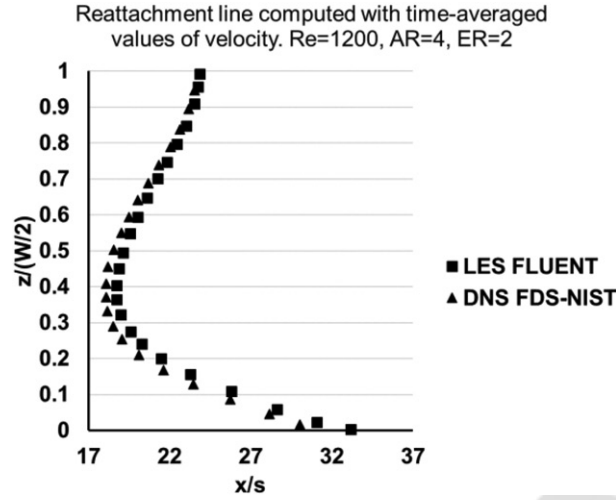


Figure 1. Comparison of results obtained with DNS (mesh size: 1.134×10^8) and LES with Dynamic Smagorinsky SGS model (mesh size: 4.08×10^6).

The convergence criterion was set so that the residuals for mass, velocity, and energy must be lower than $1E-5$. A statistically steady state is reached and, at that point, the mass imbalance reached between the inlet and outlet is less than 0.1%.

The data sampling for time statistics begins after a number of residence times in the domain, depending on Re, and the moving-average is performed over two to three residence times.

2.2. Physical model and boundary conditions

The geometry and characteristics of the computational domain are the same as those used by the authors in the theoretical-experimental study reported in [38]. A sketch of the geometry corresponding to the computational domain, with the nomenclature and coordinate system is shown in Figure 2. The channel has an expansion ratio $ER = H/s = 2$ (where H is the height at the outlet and s is the height of the step) and a low aspect ratio $AR = W/s = 4$ (where W is the width of the channel).

The length of the inlet channel, upstream of the step, is selected to ensure that a fully developed flow along the flow direction is obtained at the step region. Durst et al. [53] performed a detailed numerical study on the lengths necessary to obtain fully developed flows in laminar regime, and proposed the following correlation for 2D channels:

$$\frac{L_{in}}{h} = [(0.631)^{1.6} + (0.0442 \cdot Re)^{1.6}]^{1.6} \quad (2)$$

This correlation gives a value of 70.74 for $Re = 1,600$ (the largest Re used this study), which is only marginally higher than the value of 68.30 corresponding to the experimental installation used in [38], and set for the computational domain used in this study. The value of 68.30 is sufficient to ensure fully developed flow at the step, as it was verified by comparing the streamwise velocity profiles just downstream of the step, non-dimensionalized with the bulk velocity at the domain inlet, for Re equal to 1,000, 1,200, and 1,600. The three profiles coincide, which ensures that the flow at the step section corresponds to a fully developed flow for all the Re studied. Note that Re herein is defined based on the bulk velocity at the inlet of the channel and the maximum height of the channel (i.e., 2h), which is equivalent to the definition used by Armaly et al. [14].

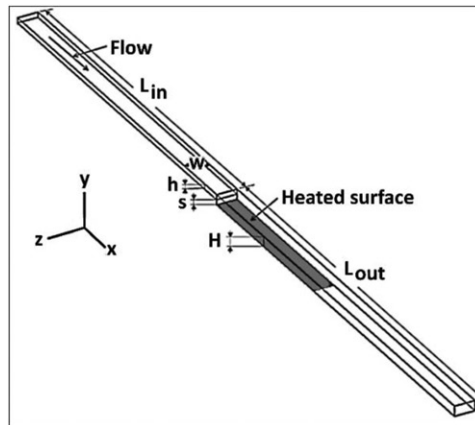


Figure 2. Computational domain.

As for the length of the channel downstream of the step, it was selected sufficiently large to remove the disturbances of the boundary condition in the exit plane on the flow variables in the zones of interest, that is, the recirculation bubbles and the region immediately downstream. The disturbances are limited to a zone close to the outlet. This length is selected as $L_{out}/s = 82$, which is longer than those used in the references cited above [16, 22, 31, 32].

The hot surface in the bottom wall downstream of the step has a length $L_{hot}/s = 34$, identical to that used in the previous theoretical-experimental study [38], which is sufficiently large to capture all the primary recirculation bubbles and a number of step lengths downstream of it for the whole range of Reynolds numbers.

At the duct inlet, uniform temperature and streamwise velocity profiles are imposed. As an ideal compressible gas is considered in this study, an outflow boundary condition, i.e., zero-gradient of all variables in the streamwise direction, cannot be imposed at the outlet plane. The pressure outlet condition (zero gauge pressure) was imposed instead.

The lower and upper walls of the channel and the step wall are considered as no-slip. However, on the sidewalls, two boundary conditions are considered: no-slip and slip (similar to periodic boundary conditions), comparing the results obtained in both simulations. This comparison is done to discriminate the 3D instabilities inherent to the flow itself from the 3D effects because of the sidewalls.

The temperature of the hot zone in the lower wall is kept constant at T_{hot} , which is greater than the inlet temperature, T_0 , for all Re studied. This yields Richardson numbers smaller than 0.02 for all cases; thus, it is concluded that this is a forced convective flow.

2.3. Mesh sensitivity analysis and model validation

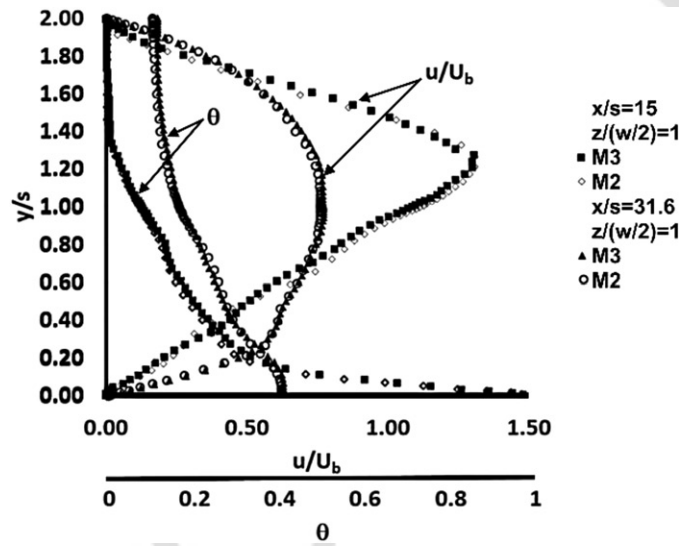
The computational domain in this study is the same as the one used by Juste and Fajardo [38], in which the authors performed a mesh independence study to ensure the independence of the results with the mesh size for $Re = 1,200$. Three mesh resolutions, with fixed inflation and the same cell growth ratio (1.2), were analyzed. The primary characteristics were reported in Table 1 of Juste and Fajardo [38]. As a result of said analysis, the M2 mesh was selected to conduct the study.

In this study, the mesh independence analysis was extended to cover the complete range of Re under consideration by comparing the results obtained for $Re = 1,600$ with meshes M2 and M3.

The meshes are hexahedral grids, and are designed to obtain a near-wall distance $y^+ < 1$ at the walls. As an example, for the case of $Re = 1,200$ and the M2 mesh in the simulation with no-slip boundary conditions in the sidewalls, this value was 0.15 for the bottom wall and 0.35 for the

Table 1. Strouhal number in a BFS flow in the Re range 1,000–1,200.

Ref.	AR	ER	Re _h	St
Rani and Sheu [16]	8	2	833	0.144
Rani and Sheu [16]	8	2	1,130	0.213
Rani and Sheu [16]	8	2	2,250	0.154
Xu et al. [33]	16	2	1,000	0.122
Xu et al. [33]	16	2	1,200	0.117
Xu et al. [33]	16	2	1,400	0.128
Xie and Xi [31]	2D	2	2,000	0.058
This study (slip)	4	2	1,000	0.156
This study (slip)	4	2	1,100	0.14
This study (slip)	4	2	1,150	0.161
This study (slip)	4	2	1,200	0.177
This study (slip)	4	2	1,400	0.174

**Figure 3.** Streamwise velocity and no-dimensional temperature profiles at two different locations ($x/s = 15$ and 31.6) for the two meshes considered in the mesh independence study.

side and upper walls. For the same mesh, M2, and $Re = 1,600$, the value is less than 0.5 in all the walls of the computational domain.

Figure 3 shows a sample of the results obtained for $Re = 1,600$, comparing the streamwise velocity and dimensionless temperature, defined as $\theta = (T - T_0)/(T_{hot} - T_0)$, profiles. The profiles are obtained at two streamwise positions ($x/s = 15$ and 31.6) in the midplane of the channel. In both cases, the profiles obtained are approximately overlapping, with an insignificant variation in the region of the primary recirculation bubble. Considering the aim of this study, these differences do not justify the increase in computational cost of using the M3 mesh ($1E7$ cells); therefore, the M2 mesh, with $4E6$ cells, was used for all numerical simulations in this study.

The numerical model used in this study was validated in [37] for an adiabatic flow case against benchmarked results by Armaly et al. [6] and further qualitatively compared against the experimental results and also, with the numerical results [37], obtained with another well-established LES code for low Mach numbers [52]. When heat transfer through the bottom wall is considered [38], the numerical model was compared with the results obtained by Nie and Armaly [14], who performed a study for a geometry with $ER = 2$ and $AR = 8$ for Re in the laminar regime, and assuming a uniform heat flow at the heating wall. Figure 4 shows a summary of the validation for this case with heat transfer. The agreement found is good for both the reattachment line and

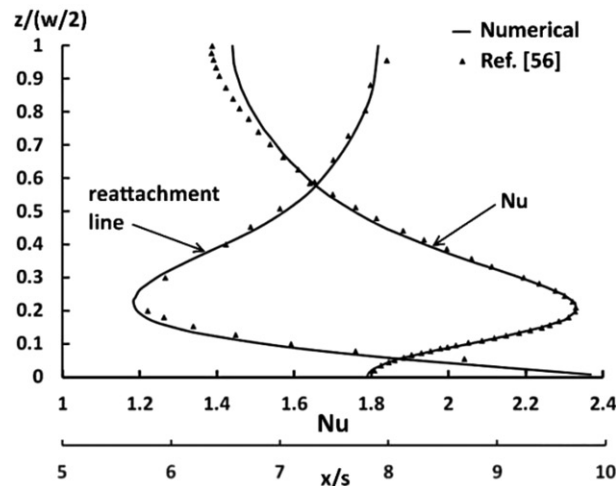


Figure 4. Comparison of the reattachment line and Nu distribution obtained numerically with those obtained by Nie and Armary [13].

the spanwise distribution of the Nu, except in the central region of the channel, where there are small differences.

3. Flow field analysis

The primary aim of this study is to determine the maximum Re for which the 3D flow effects from the presence of the lateral walls are dominant over the intrinsic 3D flow instabilities, and then analyze their impact on the heat transfer characteristics in a low aspect ratio BFS. More specifically, said 3D flow effects are the wall-jets and the secondary recirculation bubble in the upper wall, confined in a region next to the sidewalls, and their effect on the reattachment line.

As previously mentioned, to isolate the effect of the sidewalls, the flow with heat transfer is analyzed for both imposed slip and no-slip sidewalls.

Firstly, the evolution of the flow topology with the Re is studied in the case of slip sidewalls, observing when 3D features begin to appear exclusively because of the intrinsic instabilities that emerge when a critical value of the bifurcation parameter is reached. Upon reaching that condition, the quasi-steady flow transitions fully into a chaotic flow. This solution is then compared against the one with no-slip boundary conditions in the sidewalls.

Finally, the influence of the different flow topologies on the heat transfer characteristics in the region of the bottom wall downstream of the step containing the primary recirculation bubble, in the mixed-forced convective flow case, is analyzed.

3.1. Analysis of slip sidewalls

Figure 5 shows the iso-contours of the instantaneous streamwise velocity in the midplane of the channel (left), and in a horizontal plane ($y/s = 0.083$) close to the bottom wall (right), for the case of slip sidewalls. As can be seen in the figure, for Re smaller than 1,000, the flow is 2D, with the average values and the instantaneous ones approximately coincident. For $Re = 1,000$, very weak regions of negative velocity begin to appear in the bottom and top of the channel, downstream of the recirculation bubbles. These instabilities correspond to vortical structures that originate downstream of the primary (lower) and secondary (upper) bubbles. The regions of negative velocity are separated from the main recirculation bubbles and move down until they mix with the main

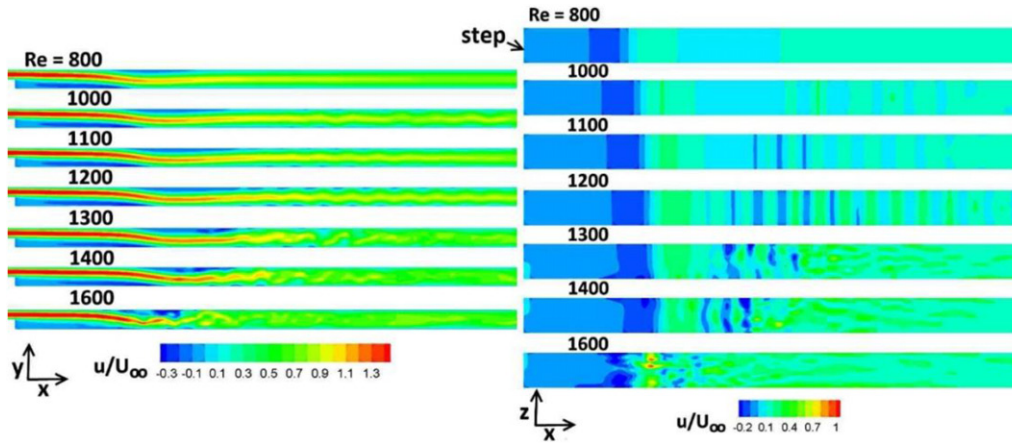


Figure 5. Iso-contours of instantaneous streamwise velocity in the midplane of the channel (left) and a horizontal plane ($y/s = 0.083$) close to the bottom wall (right), for various Re , with slip sidewalls.

stream and disappear. In this process, the reattachment line moves slightly downstream with time until these vortical structures begin to appear and the reattachment line then jumps upstream, leading to quasi-periodic oscillations of the line. This phenomenon is known in the literature as flapping of the reattachment line.

As Re increases, the reattachment line moves downstream and the upper recirculation bubble increases in size. It also increases the intensity and size of the seeded vortices downstream of the step, as well as the amplitude of the oscillations of the reattachment points.

The recirculation bubbles developing downstream of the main recirculation bubbles have a 3D character. The vortical structures grow spirally, generating small velocity components in the spanwise direction, and breaking the flow two-dimensionality. These phenomena can be seen in [Figure 6](#) (top), where the flow stream traces for a number of Re numbers are shown. As the sidewalls are modeled as slip walls, it is apparent that these 3D flows are not caused by the presence of lateral walls, but because of an intrinsic 3D flow instability over the BFS.

However, up to Re numbers in the range 1,150–1,200, the topology of the flow exhibits a quasi-2D behavior, except for the small spanwise flows in the vortex regions, as can be seen in [Figure 6](#) (bottom), which shows the iso-contours of the standardized Q -criterion [54] for the studied Re . For $Re = 1,200$, the flow three-dimensionality appears, and a fully 3D chaotic flow can be seen clearly for $Re = 1,600$.

This result can also be verified using another method to identify the vortices, depicting the vortex core lines around which the spiral flows of the vortical structures are developed ([Figure 7](#)). The lines are computed with the lambda-2 method developed by Jeong and Hussain [55]. Once again, for $Re \geq 1,200$, the flow begins to lose the quasi-2D configuration, which is clearly evident above $Re = 1,300$. The flow acquires a fully chaotic behavior at $Re = 1,600$, as shown in [Figure 6](#) by the stream traces and Q -criterion, and in [Figure 7](#) by the vortex core lines. As mentioned above, this three-dimensionality cannot be because of the effect of the sidewalls.

The possible mechanisms of generation of the vortical structures has been studied in detail by authors such as Barkley et al. [20], who reported an essentially centrifugal mechanism, 3D in nature, within the primary recirculation region, associated with closed streamlines close to the walls.

On the other hand, other researchers, such as Lanzerstorfer et al. [23], reported that, for a BFS with $ER = 2$, the instability is because of a combination of the flow deceleration close to the reattachment point, a lift-up process on both sides of the main flow between the primary and secondary recirculation bubbles, and an amplification because of the convergence of the streamlines close to the separated regions.

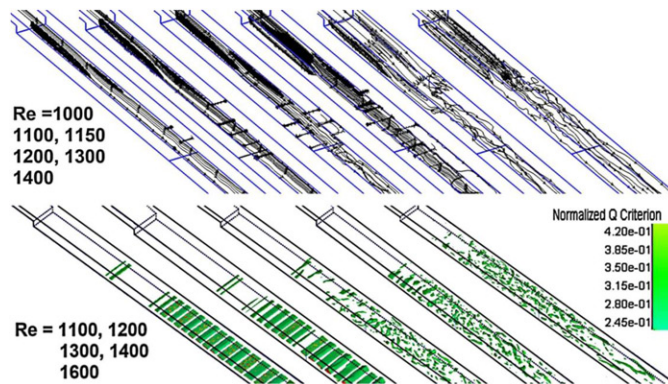


Figure 6. Flow stream traces (top) and iso-contours of the standardized Q-criterion (bottom) for the Re range under study.

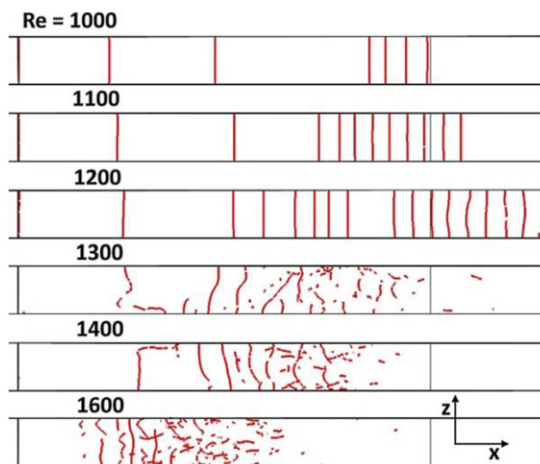


Figure 7. Vortex core lines in the domain, calculated using the lambda-2 method developed by Jeong and Hussain [55].

Although it is not an objective of this work, the study of the mechanism of formation of those vortical structures that emerge from the main recirculation regions and travel convectively downstream was investigated. Figure 8 presents a visualization of the streaklines generated from the injection of massless particles at a number of points on a vertical line located downstream of the step, in the midplane of the channel, for the $Re = 1,200$ case. The first three images in Figure 8 represent the streaklines generated from injection points close to the bottom wall, and the last three images from injection points close to the upper wall. In these plots, the evolution of the streaklines is represented together with the iso-contours of the streamwise velocity in the midplane at three different times. It can be clearly seen that the streaklines emerge from the interaction of the shear layer with the recirculation regions. The streaklines roll up increasingly, causing a growth in the negative axial velocity regions and the consequent flapping of the reattachment line. These regions of negative flow, which are convected downstream, correspond to the previously mentioned vortical structures represented by vortex core lines that are linked to the oscillations of the primary and secondary bubbles.

These numerical results were qualitatively confirmed experimentally through smoke visualization tests for $Re = 1,200$ in a BFS with $ER = 2$, but with $AR = 8$, as shown in the last image in Figure 8 for the midplane of the channel. Although it does not coincide quantitatively, as there is a residual effect of the sidewalls in the experimental facility that disturbs the flow, the qualitative agreement is good, and the roll-up process of the streaklines, both in the upper and lower parts of the channel, can be clearly seen.

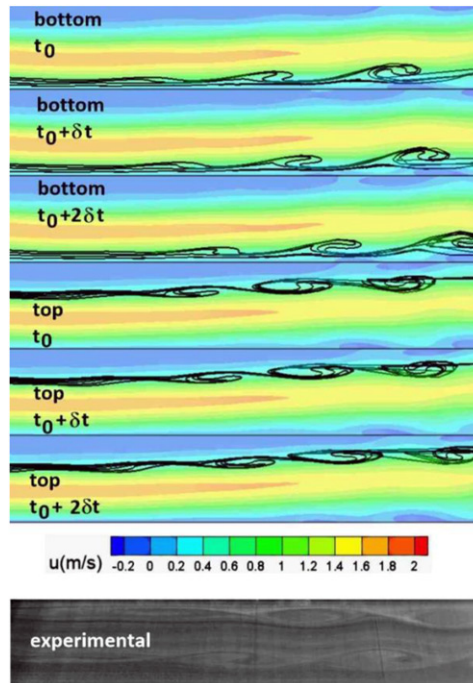


Figure 8. Streaklines generated from the injection of massless particles at a number of points on a vertical line located downstream of the step, in the lower part of the channel (labeled “bottom”) and in the upper part of the channel (labeled “top”), plotted over the iso-contours of streamwise velocity in the midplane of the channel ($Re = 1,200$). The last image depicts smoke lines at the midplane from experimental tests.

The observed rolling-up process is quasi-periodic, as can be verified by acquiring temporary samples of the velocities at different flow field points and calculating the fast Fourier transform (FFT) of these data. Figure 9 shows one of these computed FFT of the u and v components of the velocity at a point in the central z -plane and at the lower part of the channel, downstream of the primary recirculation bubble for the cases with $Re = 1,200$ and $Re = 1,600$. For $Re = 1,200$, a dominant frequency peak can be detected. However, for $Re = 1,600$, multiple frequency peaks appear. This second condition corresponds to a more chaotic movement, as shown in Figure 6 (bottom) and Figure 7, where the Q -criterion and the vortex core lines are represented, respectively. These dominant frequencies correspond to Strouhal numbers of order 0.1. Table 1 presents the St for $Re = 1,000$ to $Re = 1,400$, comparing it with the results of other researchers.

The results obtained agree in order of magnitude with the results published in the literature, however, a detailed comparison is difficult because of a number of factors, such as the different geometries used, boundary conditions upstream of the step and in the sidewalls, as well as the possible influence of the heat transfer in the bottom wall on the frequency of the vortex shedding and, therefore, on the Re - St relationship [56]. Additionally, different numerical schemes were used in each study.

3.2. Analysis of no-slip sidewalls

With the no-slip boundary condition in the sidewalls, the flow topology changes radically because of the influence of the lateral walls. In the midplane, the flow structure is similar to that of the case with slip sidewalls, as can be seen in Figure 10 (left), where the instantaneous streamwise velocity iso-contours in the midplane for various Re are shown. The influence of the sidewalls is clearly seen in Figure 10 (right), where the instantaneous streamwise velocity iso-contours are

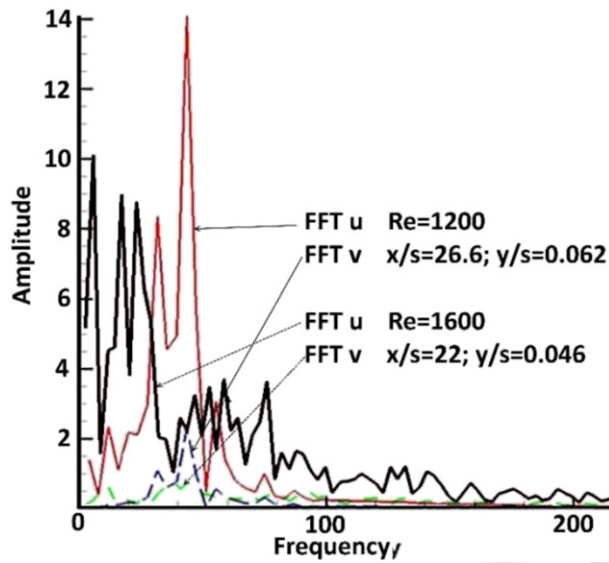


Figure 9. FFT of u and v velocity components at a point in the central z -plane and at the lower part of the channel for $Re = 1,200$ and $Re = 1,600$, in the case of slip sidewalls.

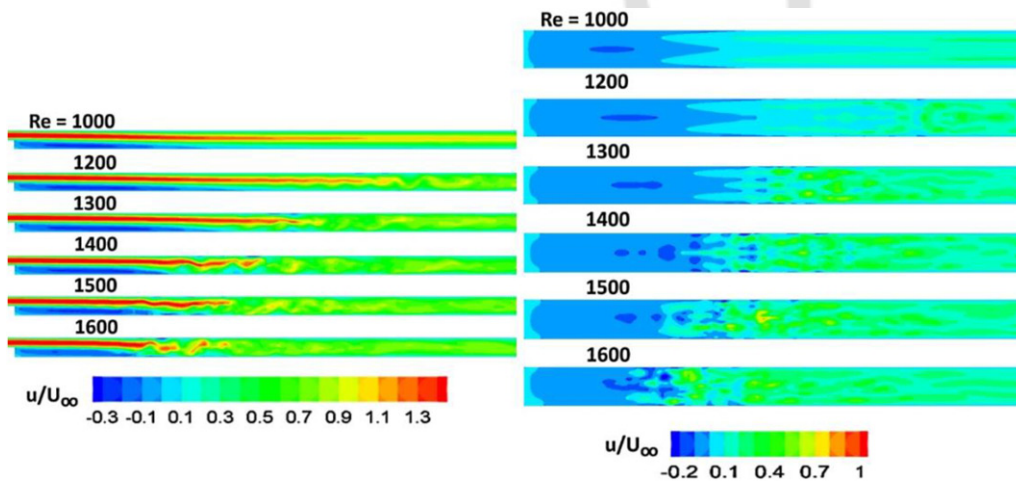


Figure 10. Instantaneous streamwise velocity iso-contours in the midplane of the channel (left) and in a horizontal plane ($y/s = 0.08$) close to the bottom wall (right) for various Re in the no-slip sidewalls case.

also shown for the same Re values in a plane $y/s = 0.08$ (i.e., close to the bottom wall). The reattachment line has maximum values in the center of the channel and close to the sidewalls because of the influence of the wall-jets. The wall-jets are the flows moving from the wall to the center of the channel, generated by the effect of the wall in a region of sudden expansion, that enhance the primary recirculation bubble close to the midplane. The wall-jets can be seen more clearly in Figure 11, where the streamlines are shown for the case $Re = 1,200$ in perspective and in the zx - and xy -planes. In this figure, the primary and secondary recirculation bubbles can also be seen. As opposed to what was found for the slip sidewalls case, the secondary bubble does not cover the entire width of the channel for the no-slip sidewalls condition, being confined in a region close to the sidewalls and, therefore, strengthening the wall-jets.

The main recirculation bubbles, both the upper and the lower, grow in size as the Re increases. The flow is therefore 3D, but symmetrical with respect to the midplane up to Re of the order of

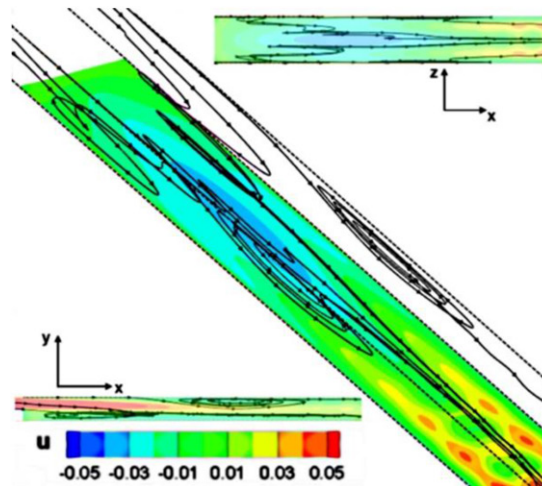


Figure 11. Flow streamlines for the case with $Re = 1,200$, in perspective and in the zx - and xy -planes, clearly showing the wall-jets.

1,400. As the Re continues to increase, this symmetric configuration of the flow is lost, decreasing the average value of the distance from the step to the reattachment line.

The 3D effects because of the sidewalls, and the symmetrical configuration of the flow, become increasingly evident in the vortex core lines (Figure 12, left) and iso-contours of Q -criterion (Figure 12, right). In these figures, the symmetry of the flow in the region close to, and downstream of the step, is clearly shown. It can be seen that the symmetry downstream of the step disappears when Re increases, completely vanishing for Re numbers at approximately 1,500. Comparing these results against those obtained with slip sidewalls highlights the influence of the lateral walls on the flow pattern. The existence of no-slip sidewalls results in a symmetric flow configuration being maintained for Re values significantly greater than the critical value for which the intrinsic 3D instabilities dominate, established at approximately 1,200 according to the patterns shown in Figures 6 and 7.

In the midplane of the channel, there remains a certain periodicity of the flow downstream of the primary recirculation bubble, as well as in regions close to the bottom wall, as shown in Figure 13, where the FFT of the streamwise and spanwise components of the velocity are plotted for $Re = 1,200$. The dominant frequency peak appears with a value similar to the one obtained in the case with slip walls; however, it has a significantly lower amplitude. Moving away from the midplane, the effects induced by the sidewalls overlap with the intrinsic 3D instabilities, masking those effects inherent to the flow itself.

4. Heat transfer characteristics analysis

The effect induced by the sidewalls is a modification of the heat transfer characteristics in the heated lower wall of the BFS. The intrinsic flow instabilities modify the thermal boundary layer, enhancing the heat transfer in the regions corresponding to the vortex shedding, downstream of the recirculation bubble. Figure 14 shows iso-contours of the Nu in the bottom heated wall for a number of Re values, in both the slip and no-slip sidewall cases, together with the reattachment lines in a plane adjacent to the bottom wall. For Re larger than 1,000, when the vortical structures form, Nu peaks, located in quasi-2D regions corresponding to these vortical structures, arise. The 2D configuration begins to disappear for Re numbers greater than approximately 1,300. These Nu peaks are seen more clearly in Figure 15, where the spanwise-averaged values of the instantaneous Nu are compared for several Re in the case of slip and no-slip sidewalls, as a function of

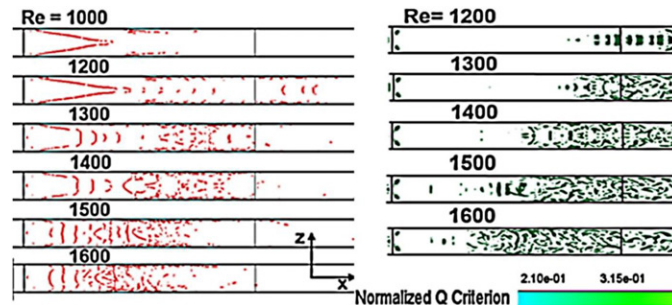


Figure 12. Vortex core lines (left) and iso-contours of Q-criterion (right) for different Re with no-slip sidewalls.

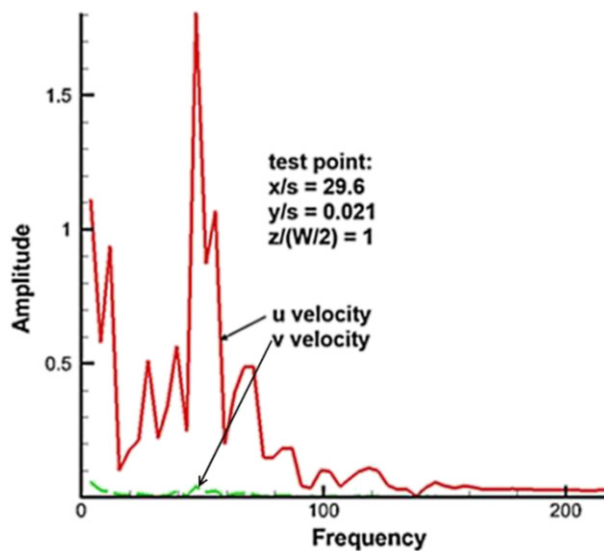


Figure 13. FFT of the streamwise and spanwise components of velocity, with no-slip sidewalls, for Re = 1,200.

x (streamwise coordinate). A first peak of the Nu is identified, which corresponds to the primary recirculation bubble. For Re greater than 1,000, a number of Nu value peaks then appear, which correspond to the vortical structures that emerge from the primary recirculation bubble and travel downstream. This effect is less noticeable for Re = 1,000, where the instantaneous and time-averaged Nu coincide in the bulk of the hot plate, but it becomes more evident with increasing Re, as these vortical structures become stronger. The final result is an increase in the time-averaged value of the Nu.

The situation is somewhat different in the case of no-slip sidewalls. Figure 14 (right) shows the iso-contours of the Nu in the heated lower wall. The maximum values of Nu appear symmetrically in areas close to the lateral walls, where the reattachment length is smallest. As Re increases, these points, where the maximum Nu is reached, are moved downstream, up to a value of Re of approximately 1,400, when the flow is still symmetrical and dominated by the effect of the sidewalls. From that point onwards, the intrinsic 3D instabilities begin to appear. For Re = 1,600, the symmetry of the flow has completely disappeared, and the flow is fully chaotic.

The final result is a span-averaged Nu distribution in the streamwise direction that provides lower values in the no-slip sidewalls case (Figure 15). The difference is more noticeable for low Re (1,000–1,200), corresponding to the beginning of transitional flow regime, where the vortical structures begin to appear but their effects are masked by the influence of the sidewalls. This difference between the two values of the Nu decreases as Re increases and the flow becomes more

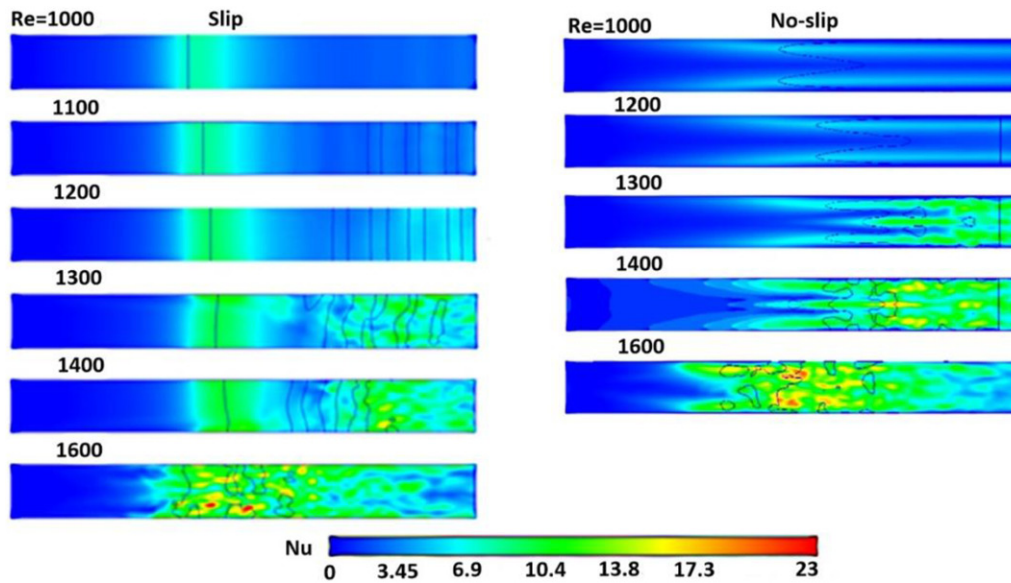


Figure 14. Iso-contours of the Nu in the lower wall for several Re in both the slip (left) and no-slip (right) sidewall cases. Black lines indicate the position of the reattachment line.

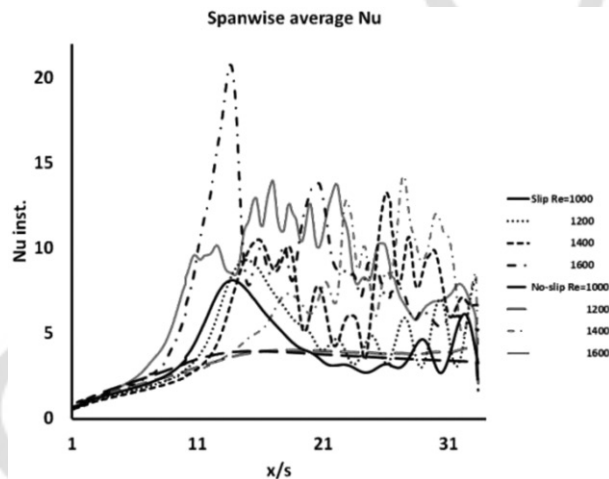


Figure 15. Evolution of spanwise-averaged values of the instantaneous Nu and time-averaged values for several Re in both the slip and no-slip sidewall cases.

turbulent. In the turbulent regime, the effect of the side walls on the average heat transfer in the bottom wall tends to disappear.

Figure 16 shows the evolution of the time-averaged mean Nu of the entire hot plate immersed in the recirculation bubble with the flow Re. As the intrinsic instabilities appear in the slip sidewalls case, transitional flow begins. There is an abrupt change in slope, increasing the Nu and, therefore, the heat transfer. However, in the no-slip case, the effect of the vortical structures on the heat transfer is dampened by the induced effect of the sidewalls through the wall-jets that penetrate towards the midplane. As Re increases, the Nu increases in both cases. However, the difference between both decreases as Re increases and the flow evolves towards a fully chaotic structure, where the effect induced by the sidewalls ceases to be dominant.

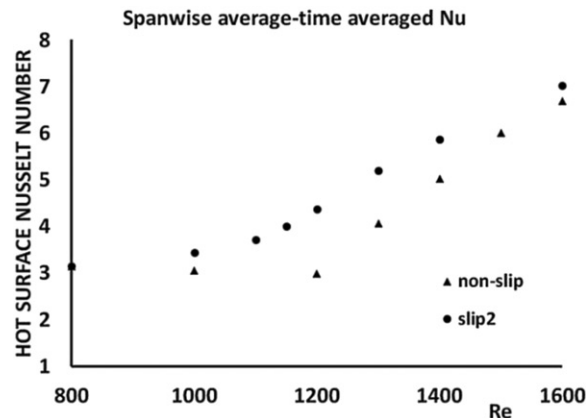


Figure 16. Evolution of time-averaged mean Nu of the entire hot plate immersed in the recirculation bubble with the flow Re for both sidewall conditions.

5. Conclusions

This research studies the influence of the existence of lateral walls on heat transfer phenomena and the intrinsic instabilities in the flow over a narrow rectangular duct ($AR = 4$) with a BFS. The study is performed in the transitional regime for a Re range 1,000–1,600, where the intrinsic flow 3D instabilities become dominant, inducing a chaotic flow behavior. The main aim was to identify up to what Re value 3D flows induced by the presence of the sidewalls would effectively mask the intrinsic three-dimensional instabilities of detached and reattached flows; and the influence on the heat transfer characteristics in the bottom wall, both of the three-dimensional flows due to the geometry with low aspect ratio of the BFS and of the intrinsic 3D instabilities of the flow.

The study was conducted using LES, with the Dynamic Smagorinsky formulation. To differentiate the three-dimensionality of the flow because of the geometry in channels with small aspect ratios from the intrinsic 3D instability of a separated and reattached flow, as found over the BFS, two types of numerical simulations were carried out, the first with slip boundary conditions on the sidewalls, the second with boundary conditions corresponding to the actual configuration of the BFS. The mesh-independence of the results was verified for the largest Re under investigation.

The numerical simulations indicate that the flow topology in the case with slip sidewalls exhibits 3D features that begin to appear exclusively because of the intrinsic instabilities that emerge when a critical value of the bifurcation parameter is reached. These instabilities, in the form of vortical structures, appear for the first time at a Re of approximately 1,000 in both the upper and lower region of the channel. They subsequently detach from the primary and secondary recirculation bubbles, inducing flapping of the reattachment line, and are convected downstream in a roll-up process. As Re increases, the reattachment line moves downstream and the upper recirculation bubble grows, also increasing the intensity of the vortex shedding. Up to a Re of the order of 1,150–1,200, the flow field is still quasi-bidimensional. At $Re = 1,300$, it is clear that the flow has lost its quasi-bidimensionality, and at approximately $Re = 1,600$ the flow is fully 3D and chaotic. For the case of low Re, the process is quasi-periodic and a dominant frequency is found, while at larger Re the flow becomes chaotic, resulting in multiple frequency peaks.

No-slip sidewalls produce radical changes in the flow topology. The flow differs significantly, primarily because of the effect of the wall-jets, which mask three-dimensional intrinsic instabilities at the beginning of transitional regime. In this case, the upper recirculation bubble does not cover the complete channel span and, therefore, the flow is not 2D, even at low Re. However, the

flow remains symmetrical beyond the critical value of the bifurcation parameter found for the slip sidewalls condition, up to a Re of approximately 1,400, losing the symmetry and acquiring a chaotic behavior for greater Re values. Regarding the periodicity of the flow, there remains a dominant frequency in the midplane with a similar value to the one obtained for the slip sidewalls case, however, this periodicity is lost away from the midplane.

When the heat transfer in the bottom wall next to and downstream of the step wall is studied, it is detected that, for low Re , the largest value of Nu is found in the flow area where the reattachment line is closest to the step wall. This occurs near the lateral walls in the no-slip boundary conditions case, and next to reattachment line in the slip sidewalls case. However, these structures disappear when the flow transitions into a fully chaotic flow for $Re = 1,600$, when the intrinsic flow instabilities become dominant. The evolution of Nu with the streamwise distance shows several peaks, corresponding to the vortical structures, resulting in a net increase in the time-averaged mean value of the Nu on the hot bottom surface.

ORCID



G. L. Juste  <http://orcid.org/0000-0002-7663-9084>

M. C. Espino  <http://orcid.org/0000-0002-0531-8021>

References

- [1] A. Dewan and P. Srivastava, "A review of heat transfer enhancement through flow disruption in a micro-channel," *J. Therm. Sci.*, vol. 24, no. 3, pp. 203–214, 2015. DOI: [10.1007/s11630-015-0775-1](https://doi.org/10.1007/s11630-015-0775-1).
- [2] X. Liu, G. Zhang, B. Sunden, and G. Xie, "Numerical predictions of flow and heat transfer of film cooling with an internal channel roughened by crescent ribs," *Numer. Heat Transf. Part A: Appl.*, vol. 74, no. 9, pp. 1539–1564, 2018. DOI: [10.1080/10407782.2018.1538291](https://doi.org/10.1080/10407782.2018.1538291).
- [3] A. Abdelmoula, B. A. Younis, S. Spring, and B. Weigand, "Large-eddy simulations of heated flows in ribbed channels with spanwise rotation," *Numer. Heat Transf. Part A Appl.*, vol. 74, no. 1, pp. 895–916, 2018. DOI: [10.1080/10407782.2018.1513282](https://doi.org/10.1080/10407782.2018.1513282).
- [4] M. K. Denham and M. A. Patrick, "Laminar flow over a downstream-facing step in a two-dimensional flow channel," *Trans. Inst. Chem. Eng.*, vol. 52, pp. 361–367, 1974.
- [5] J. K. Eaton and J. P. Johnston, "A review of research on subsonic turbulent flow reattachment," *AIAA J*, vol. 19, no. 9, pp. 1093–1100, 1981. DOI: [10.2514/3.60048](https://doi.org/10.2514/3.60048).
- [6] B. F. Armaly, F. Durst, J. C. F. Pereira, and B. Schönung, "Experimental and theoretical investigation of backward-facing step flow," *J. Fluid Mech.*, vol. 127, no. 1, pp. 473–496, 1983. DOI: [10.1017/S0022112083002839](https://doi.org/10.1017/S0022112083002839).
- [7] P. T. Williams and A. J. Baker, "Numerical simulations of laminar flow over a three-dimensional backward-facing step," *Int. J. Numer. Methods Fluid*, vol. 24, no. 11, pp. 1159–1183, 1997. DOI: [10.1002/\(SICI\)1097-0363\(19970615\)24:11<1159::AID-FLD534>3.0.CO;2-R](https://doi.org/10.1002/(SICI)1097-0363(19970615)24:11<1159::AID-FLD534>3.0.CO;2-R).
- [8] T. P. Chiang and T. W. Sheu, "A numerical revisit of backward-facing step flow problem," *Phys. Fluids*, vol. 11, no. 4, pp. 862–874, 1999. DOI: [10.1063/1.869958](https://doi.org/10.1063/1.869958).
- [9] G. Biswas, M. Breuer, and F. Durst, "Backward-facing step flows for various expansion ratios at low and moderate Reynolds numbers," *J. Fluids Eng.*, vol. 126, no. 3, pp. 362–374, 2004. DOI: [10.1115/1.1760532](https://doi.org/10.1115/1.1760532).
- [10] J. Tihon, V. Pěnkavová, and M. Pantzali, "The effect of inlet pulsations on the backward-facing step flow," *Eur. J. Mech. B Fluids*, vol. 29, no. 3, pp. 224–235, 2010. DOI: [10.1016/j.euromechflu.2010.02.001](https://doi.org/10.1016/j.euromechflu.2010.02.001).
- [11] N. Tylli, L. Kaiktsis, and B. Ineichen, "Sidewall effects in flow over a backward-facing step: Experiments and numerical simulations," *Phys. Fluids*, vol. 14, no. 11, pp. 3835–3845, 2002. DOI: [10.1063/1.1506163](https://doi.org/10.1063/1.1506163).
- [12] N. A. Malamataris, "A numerical investigation of wall effects in three-dimensional, laminar flow over a backward facing step with a constant aspect and expansion ratio," *Int. J. Numer. Methods Fluid*, vol. 71, no. 9, pp. 1073–1102, 2013. DOI: [10.1002/flid.3699](https://doi.org/10.1002/flid.3699).
- [13] H. Iwai, K. Nakabe, and K. Suzuki, "Flow and heat transfer characteristics of backward-facing step laminar flow in a rectangular duct," *Int. J. Heat Mass Transf.*, vol. 43, no. 3, pp. 457–471, 2000. DOI: [10.1016/S0017-9310\(99\)00140-4](https://doi.org/10.1016/S0017-9310(99)00140-4).
- [14] B. F. Armaly, A. Li, and J. H. Nie, "Measurements in three-dimensional laminar separated flow," *Int. J. Heat Mass Transf.*, vol. 46, no. 19, pp. 3573–3582, 2003. DOI: [10.1016/S0017-9310\(03\)00153-4](https://doi.org/10.1016/S0017-9310(03)00153-4).

- [15] J. H. Nie, B. F. Armaly, and B. F. “Reverse flow regions in three-dimensional backward-facing step flow,” *Int. J. Heat Mass Transf.*, vol. 47, no. 22, pp. 4713–4720, 2004. DOI: [10.1016/j.ijheatmasstransfer.2004.05.027](https://doi.org/10.1016/j.ijheatmasstransfer.2004.05.027).
- [16] H. P. Rani and T. W. Sheu, “Nonlinear dynamics in a backward-facing step flow,” *Phys. Fluids*, vol. 18, no. 8, pp. 084101, 2006. DOI: [10.1063/1.2261852](https://doi.org/10.1063/1.2261852).
- [17] H. P. Rani, T. W. Sheu, and E. S. Tsai, “Eddy structures in a transitional backward-facing step flow,” *J. Fluid Mech.*, vol. 588, pp. 43–58, 2007. DOI: [10.1017/S002211200700763X](https://doi.org/10.1017/S002211200700763X).
- [18] T. W. Sheu and H. P. Rani, “Exploration of vortex dynamics for transitional flows in a three-dimensional backward-facing step channel,” *J. Fluid Mech.*, vol. 550, no. 1, pp. 61–83, 2006. DOI: [10.1017/S0022112005007858](https://doi.org/10.1017/S0022112005007858).
- [19] L. Kaiktsis, G. E. Karniadakis, and S. A. Orszag, “Onset of three-dimensionality, equilibria, and early transition in flow over a backward-facing step,” *J. Fluid Mech.*, vol. 231, pp. 501–528, 1991. DOI: [10.1017/S0022112091003488](https://doi.org/10.1017/S0022112091003488).
- [20] D. Barkley, M. G. M. Gomes, and R. D. Henderson, “Three-dimensional instability in flow over a backward-facing step,” *J. Fluid Mech.*, vol. 473, pp. 167–190, 2002. DOI: [10.1017/S002211200200232X](https://doi.org/10.1017/S002211200200232X).
- [21] J. F. Beaudoin, O. Cadot, J. L. Aider, and J. E. Wesfreid, “Three-dimensional stationary flow over a backward-facing step,” *Eur. J. Mech. B Fluid*, vol. 23, no. 1, pp. 147–155, 2004. DOI: [10.1016/j.euromechflu.2003.09.010](https://doi.org/10.1016/j.euromechflu.2003.09.010).
- [22] H. M. Blackburn, D. Barkley, and S. J. Sherwin, “Convective instability and transient growth in flow over a backward-facing step,” *J. Fluid Mech.*, vol. 603, pp. 271–304, 2008. DOI: [10.1017/S0022112008001109](https://doi.org/10.1017/S0022112008001109).
- [23] D. Lanzerstorfer and H. C. Kuhlmann, “Global stability of the two-dimensional flow over a backward-facing step,” *J. Fluid Mech.*, vol. 693, pp. 1–27, 2012. DOI: [10.1017/jfm.2011.399](https://doi.org/10.1017/jfm.2011.399).
- [24] F. Schäfer, M. Breuer, and F. Durst, “The dynamics of the transitional flow over a backward-facing step,” *J. Fluid Mech.*, vol. 623, pp. 85–119, 2009. DOI: [10.1017/S0022112008005235](https://doi.org/10.1017/S0022112008005235).
- [25] D. Wee, T. Yi, A. Annaswamy, and A. F. Ghoniem, “Self-sustained oscillations and vortex shedding in backward-facing step flows: simulation and linear instability analysis,” *Phys. Fluids*, vol. 16, no. 9, pp. 3361–3373, 2004. DOI: [10.1063/1.1773091](https://doi.org/10.1063/1.1773091).
- [26] T. Kondoh, Y. Nagano, and T. Tsuji, “Computational study of laminar heat transfer downstream of a backward-facing step,” *Int. J. Heat Mass Transf.*, vol. 36, no. 3, pp. 577–591, 1993. DOI: [10.1016/0017-9310\(93\)80033-Q](https://doi.org/10.1016/0017-9310(93)80033-Q).
- [27] J. H. Nie and B. F. Armaly, “Reattachment of three-dimensional flow adjacent to backward-facing step,” *J. Heat Transf.*, vol. 125, no. 3, pp. 422–428, 2003. DOI: [10.1115/1.1571091](https://doi.org/10.1115/1.1571091).
- [28] H. Lan, B. F. Armaly, and J. A. Drallmeier, “Three-dimensional simulation of turbulent forced convection in a duct with backward-facing step,” *Int. J. Heat Mass Transf.*, vol. 52, no. 7-8, pp. 1690–1700, 2009. DOI: [10.1016/j.ijheatmasstransfer.2008.09.022](https://doi.org/10.1016/j.ijheatmasstransfer.2008.09.022).
- [29] H. Barrios-Pina, S. Viazzo, and C. Rey, “A numerical study of laminar and transitional mixed convection flow over a backward-facing step,” *Comput. Fluids*, vol. 56, pp. 77–91, 2012. DOI: [10.1016/j.compfluid.2011.11.016](https://doi.org/10.1016/j.compfluid.2011.11.016).
- [30] L. Chen, K. Asaia, T. Nonomuraa, G. Xib, and T. Liuc, “A review of backward-facing step (BFS) flow mechanisms, heat transfer and control,” *Therm. Sci. Eng. Prog.*, vol. 6, pp. 194–216, 2018. DOI: [10.1016/j.tsep.2018.04.004](https://doi.org/10.1016/j.tsep.2018.04.004).
- [31] W. A. Xie, and G. N. Xi, “Fluid flow and heat transfer characteristics of separation and reattachment flow over a backward-facing step,” *Int. J. Refrig.*, vol. 74, pp. 177–189, 2017. DOI: [10.1016/j.ijrefrig.2016.10.006](https://doi.org/10.1016/j.ijrefrig.2016.10.006).
- [32] W. A. Xie, G. N. Xi, and M. B. Zhong, “Effect of the vortical structure on heat transfer in the transitional flow over a backward-facing step,” *Int. J. Refrig.*, vol. 74, pp. 465–474, 2017. DOI: [10.1016/j.ijrefrig.2016.11.001](https://doi.org/10.1016/j.ijrefrig.2016.11.001).
- [33] J. H. Xu, S. Zou, K. Inaoka, and G. N. Xi, “Effect of Reynolds number on flow and heat transfer in incompressible forced convection over a 3D backward-facing step,” *Int. J. Refrig.*, vol. 79, pp. 164–175, 2017. DOI: [10.1016/j.ijrefrig.2017.04.012](https://doi.org/10.1016/j.ijrefrig.2017.04.012).
- [34] J. G. Barbosa Saldana, N. K. Anand, and V. Sarin, “Numerical simulation of mixed convective flow over a three-dimensional horizontal backward facing step,” *J. Heat Transf.*, vol. 127, no. 9, pp. 1027–1036, 2005. DOI: [10.1115/1.2005272](https://doi.org/10.1115/1.2005272).
- [35] R. V. R. Avancha and R. H. Pletcher, “Large eddy simulation of the turbulent flow past a backward-facing step with heat transfer and property variations,” *Int. J. Heat Fluid Flow*, vol. 23, no. 5, pp. 601–614, 2002. DOI: [10.1016/S0142-727X\(02\)00156-X](https://doi.org/10.1016/S0142-727X(02)00156-X).
- [36] P. Zhao, Z. Ge, J. Zhu, J. Liu, and M. Ye, “Quasi-direct numerical simulation of forced convection over a backward facing step: effect of Prandtl number,” *Nucl. Eng. Des.*, vol. 335, pp. 374–388, 2018. DOI: [10.1016/j.nucengdes.2018.05.012](https://doi.org/10.1016/j.nucengdes.2018.05.012).
- [37] G. L. Juste, P. Fajardo, and A. Guijarro, “Assessment of secondary bubble formation on a backward-facing step geometry,” *Phys. Fluids*, vol. 28, no. 7, pp. 074106, 2016. DOI: [10.1063/1.4958723](https://doi.org/10.1063/1.4958723).

- [38] G. L. Juste and P. Fajardo, "Influence of flow tree-dimensionality on the heat transfer of a narrow channel backward facing step flows," *Int. J. Therm. Sci.*, vol. 132, pp. 234–248, 2018. DOI: [10.1016/j.ijthermalsci.2018.06.005](https://doi.org/10.1016/j.ijthermalsci.2018.06.005).
- [39] E. Shima and K. Kitamura, "New Approach of efficient and time accurate compressible CFD for unsteady low Mach Number flows," presented at the 50th AIAA Aerospace Science Meeting, AIAA, 2012. DOI: [10.2514/6.2012-571](https://doi.org/10.2514/6.2012-571).
- [40] H. Jing, L. Ru, H. Yaling, and Q. Zhiguo, "Solutions for variable density low Mach number flows with a compressible pressure-based algorithm," *Appl. Therm. Eng.*, vol. 27, no. 11-12, pp. 2104–2112, 2007. DOI: [10.1016/j.applthermaleng.2006.11.010](https://doi.org/10.1016/j.applthermaleng.2006.11.010).
- [41] T. Schneider, N. Botta, K. J. Geratz, and R. Klein, "Extension of finite volume compressible flow solvers to multi-dimensional, variable density zero Mach number flows," *Comput. Phys.*, vol. 155, no. 2, pp. 248–286, 1999. DOI: [10.1006/jcph.1999.6327](https://doi.org/10.1006/jcph.1999.6327).
- [42] J. Tyacke and P. G. Tucker, "Large eddy simulation of turbine internal cooling ducts," *Comput. Fluids*, vol. 114, pp. 130–140, 2015. DOI: [10.1016/j.compfluid.2015.02.022](https://doi.org/10.1016/j.compfluid.2015.02.022).
- [43] J. H. Ferziger and M. Peric, *Computational Methods for Fluid Dynamics*. Springer Science & Business Media, 2001.
- [44] J. Waters and D. B. Carrington, "A parallel large eddy simulation in a finite element projection method for all flow regimes," *Numer. Heat Transf. Part A Appl.*, vol. 70, no. 2, pp. 117–131, 2016. DOI: [10.1080/10407785.2016.1173453](https://doi.org/10.1080/10407785.2016.1173453).
- [45] E. Garnier, N. Adams, and P. Sagaut, *Large Eddy Simulation for Compressible Flows, Scientific Computation*. Springer, 2009.
- [46] Favre averaged Navier-Stokes equations, https://www.cfd-online.com/Wiki/Favre_averaged_Navier-Stokes_equations, 2017.
- [47] M. Germano, U. Piomelli, P. Moin, and P. W. H. Cabot, "A dynamic subgrid-scale eddy viscosity model," *Phys. Fluids*, vol. 3, no. 7, pp. 1760–1765, 1991. DOI: [10.1063/1.857955](https://doi.org/10.1063/1.857955).
- [48] D. K. Lilly, "A proposed modification of the Germano subgrid-scale closure method," *Phys. Fluid*, vol. 4, no. 3, pp. 633–636, 1992. DOI: [10.1063/1.858280](https://doi.org/10.1063/1.858280).
- [49] D. K. Tafti, "Evaluating the role of subgrid stress modeling in a ribbed duct for the internal cooling of turbine blades," *Int. J. Heat Fluid Flow*, vol. 26, no. 1, pp. 92–104, 2005. DOI: [10.1016/j.ijheatfluidflow.2004.07.002](https://doi.org/10.1016/j.ijheatfluidflow.2004.07.002).
- [50] Ansys Fluent Theory Guide, Release 17.0, ANSYS Inc., 2016.
- [51] S. E. Kim, "Large eddy simulation using unstructured meshes and dynamic subgrid-scale turbulence models," presented at the 34th Fluid Dynamics Conference and Exhibit. American Institute of Aeronautics and Astronautics, *Technical Report AIAA 2004-2548*, June 2004.
- [52] K. McGrattan, S. Hostik, J. McDermott, J. Floyd, and M. Vanella, Fire dynamics simulator technical reference guide, volume 1: Mathematical model, NIST special publication. <http://dx.doi.org/10.6028/NIST.SP.1018>, 2018.
- [53] F. Durst, S. Ray, B. Unsal, and O. A. Bayoumi, "The development lengths of laminar pipe and channel flows," *J. Fluids Eng.*, vol. 127, no. 6, pp. 1154–1160, 2005. DOI: [10.1115/1.2063088](https://doi.org/10.1115/1.2063088).
- [54] V. Kolár, "Vortex identification: New requirements and limitations," *Int. J. Heat Fluid Flow*, vol. 28, pp. 638–652, 2007.
- [55] J. Jeong, and F. Hussain, "On the identification of a vortex," *J. Fluid Mech.*, vol. 285, no. 1, pp. 69–94, 1995. DOI: [10.1017/S0022112095000462](https://doi.org/10.1017/S0022112095000462).
- [56] T. Vít, M. Ren, Z. Trávníček, F. Marsík, and C. C. M. Rindt, "The influence of temperature gradient on the Strouhal–Reynolds number relationship for water and air," *Exp. Therm. Fluid Sci.*, vol. 31, no. 7, pp. 751–760, 2007. DOI: [10.1016/j.expthermflusci.2006.08.002](https://doi.org/10.1016/j.expthermflusci.2006.08.002).